Restraint of spatial distribution in high-order harmonic generation from a model of hydrogen molecular ion*

Chang-Long Xia(夏昌龙)[1], Jun Zhang(张军)[2], Xiang-Yang Miao(苗向阳)[1,†], and Xue-Shen Liu(刘学深)[2,‡]

[1] College of Physics and Information Engineering, Shanxi Normal University, Linfen 041004, China
[2] Institute of Atomic and Molecular Physics, Jilin University, Changchun 130012, China

(Received 15 March 2017; revised manuscript received 30 March 2017; published online 6 June 2017)

The spatial distribution in high-order harmonic generation (HHG) is theoretically investigated by using a few-cycle laser pulse from a two-dimensional model of a hydrogen molecular ion. The spatial distribution in HHG demonstrates that the harmonic spectra are sensitive to the carrier envelope phase and the duration of the laser pulse. The HHG can be restrained by a pulse with the duration of 5 fs in the region from the 90th to 320th order. This characteristic is illustrated by the probability density of electron wave packet distribution. The electron is mainly located near the nucleus along the positive-x direction from 3.0 o.c. to 3.2 o.c., which is an important time to generate the HHG in the plateau area. We also demonstrate the time–frequency distribution in the region of the positive- and negative-x direction to explain the physical mechanism.

Keywords: high-order harmonic generation, spatial distribution

PACS: 32.80.Rm, 42.65.Ky, 42.65.Re **DOI:** 10.1088/1674-1056/26/7/073201

1. Introduction

High-order harmonic generation (HHG) that results from the strong nonlinear polarization induced on a gas medium by an intense laser pulse is a hot topic.[1–3] It has potential applications in strong field physics, such as obtaining a coherent soft x-ray source, generating isolated attosecond pulse,[4] tracking the electron dynamics in atoms and molecules,[5,6] and so on. The physical mechanism of the HHG can be described well by a three-step model:[7,8] ionization, acceleration, and recombination. In the process of recombination, the electron comes back near the nucleus as the electric field reverses and has certain probability to jump to the ground state and release its kinetic energy. In particular, the electron can recombine with both nuclei for H_2^+. The effect of HHG from spatial properties of electron is a hot topic.[9–12] Lambert *et al.*[13] discussed the spatial properties of harmonic generation in low order and Zhang *et al.* gave the spatial distribution in HHG from a H_2^+ and from a HeH^{2+}.[14,15] However, there is no discussion on how to restrain the spatial distribution as far as we know.

A fundamental way to control the HHG is to control the motion of an electron and its distribution in laser field. The control of electron localization has attracted a great dal of attention both theoretically and experimentally.[16–18] Roudnev *et al.*[19] proposed that the electron between nuclei can be steered by using a few-cycle pulse during the dissociation of H_2^+ and this scheme has been achieved in experiment by King *et al.*[20] Few of two-color schemes are reported to further control the electron localization.[21–23] The spatial distribution in HHG can be restrained by steering the motion of an electron cloud, e.g., if the electron is located around one of the nuclei by an intense femtosecond laser pulse, then the harmonics should mainly come from that nucleus.

Since the Hydrogen molecular ion is a simple ion, the HHG from the H_2^+ molecule has been widely discussed.[24–27] However, restraining the spatial distribution of HHG has been investigated less. In this paper, we demonstrate the spatial distribution in HHG from a model of the H_2^+ molecule. By using a few-cycle Gaussian laser pulse, the spatial HHG can be restrained by adjusting the carrier envelope phase (CEP) or the duration of the laser pulse. The spatial distribution in HHG indicates that the HHG signal is mainly from the contribution from near the nucleus along the negative-x direction with the full width at half maximum (FWHM) $\tau = 5$ fs and $\varphi = 0$. The electron is located near the nucleus in the negative-x direction. We also demonstrate the time–frequency distribution in the region of the positive- and negative-x direction to explain the physical mechanism. In addition, only a molecular ion is considered to interact with the driving pulse in our simulation, and the harmonic yields are emitted from many molecules in actual experiment.[13,28,29] The harmonic is measured after propagating for a distance and has a divergence. Our simulation just aimed to give a theoretical expectation and the resolution of HHG from which nucleus may be measured by future tech-

*Project supported by the National Natural Science Foundation of China (Grant Nos. 11504221, 61575077, 11404204, and 11447208), the Natural Science Foundation for Young Scientists of Shanxi Province, China (Grant No. 2015021023), and Program for the Top Young Academic Leaders of Higher Learning Institutions of Shanxi Province, China.

†Corresponding author. E-mail: sxxymiao@126.com
‡Corresponding author. E-mail: liuxs@jlu.edu.cn

© 2017 Chinese Physical Society and IOP Publishing Ltd

nique.

2. Theory and method

We consider a model ion of H_2^+ with Born–Oppenheimer approximation (BOA). As the laser pulse interacts with the ion, the two-dimensional Schrödinger equation can be written in atomic units as

$$\mathrm{i}\frac{\partial \Psi(x,y,t)}{\partial t} = \left[\frac{p_x^2+p_y^2}{2} + V(x,y) + xE_x(t)\right]\Psi(x,y,t). \quad (1)$$

We use soft-Coulomb potential in our simulation,

$$V(x,y) = -1/\sqrt{(x-R/2)^2+y^2+a} - 1/\sqrt{(x+R/2)^2+y^2+a}. \quad (2)$$

We set the soft-core parameter $a = 0.61$ and the distance of the two nuclei $R = 7$ a.u. to simulate a model of H_2^+, and the energy of the ground electronic state is 0.519 a.u. (including the $1/R$ nuclear repulsion). A linearly polarized few-cycle laser pulse with Gaussian envelope is chosen as $E_x(t) = E_0 f(t)\cos(\omega t+\varphi)$, where $f(t) = \exp[-4\ln(2)t^2/\tau^2]$ is the laser envelope, φ is the CEP, and τ is the full width at half maximum (FWHM). In our simulation, we suppose that the nuclei of H_2^+ are fixed at $+R/2$ and $-R/2$ along the x axis, the polarization direction of the driving pulse is also along the x axis and the propagate direction is along the z axis. Equation (1) is solved by the second-order split-operator method.[30–32] Once we obtain the wave function, the dipole acceleration can be given by the Ehrenfest theorem

$$a_x(t) = \langle \Psi(x,y,t)\left| -\frac{\partial V(x,y)}{\partial x} - E_x(t)\right|\Psi(x,y,t)\rangle. \quad (3)$$

To reveal the spatial effect, the dipole acceleration can be separated into two parts[33,34]

$$\boldsymbol{a}(t)|_{x<0} = \int_{-\infty}^{0}\left[\int_{-\infty}^{+\infty}\Psi^*(x,y,t)\left[-\frac{\partial V(x,y)}{\partial x} - E_x(t)\right]\times\Psi(x,y,t)\,\mathrm{d}y\right]\mathrm{d}x, \quad (4)$$

$$\boldsymbol{a}(t)|_{x>0} = \int_{0}^{+\infty}\left[\int_{-\infty}^{+\infty}\Psi^*(x,y,t)\left[-\frac{\partial V(x,y)}{\partial x} - E_x(t)\right]\times\Psi(x,y,t)\,\mathrm{d}y\right]\mathrm{d}x. \quad (5)$$

The relative intensity of the HHG spectrum is proportional to

$$S(\omega) \sim \left|\int \exp(-\mathrm{i}\omega t)a_x(t)\,\mathrm{d}t\right|^2. \quad (6)$$

The spatial distribution of HHG can be calculated from the dipole acceleration distribution as a function of the x coordinate as the nuclei are in the x axle[14]

$$d_{\mathrm{A}}(x,t) = \int_{-\infty}^{+\infty}\Psi^*(x,y,t)\left[-\frac{\partial V(x,y)}{\partial x} - E_x(t)\right]\times\Psi(x,y,t)\,\mathrm{d}y, \quad (7)$$

$$S(\omega,x) \sim \left|\int \exp(-\mathrm{i}\omega t)d_{\mathrm{A}}(x,t)\,\mathrm{d}t\right|^2. \quad (8)$$

3. Results and discussion

In our simulation, we choose a Gaussian envelope with the wavelength of 1600 nm, and the intensity of 3×10^{14} W/cm^2. First, we set $\tau = 6$ fs and $\varphi = 0$, the HHG spectrum with more modulations is shown by the solid line in Fig. 1. The cutoff of the HHG is around the 320th order. As is well known, the CEP of the pulse is an important parameter in few-cycle schemes. We change CEP to investigate the HHG. For the case of $\varphi = 0.3\pi$, a super-continuum plateau from the 200th order to the 310th order is obtained and the cutoff of spectrum is reduced to the 310th, as shown by the dashed line in Fig. 1. For the case of $\varphi = 0.5\pi$, the spectrum is shown by a dotted green line. Modulation around the plateau of the HHG spectrum and the cutoff is the 240th order. The maximum intensity of the laser pulse reduces as the CEP increases for the above cases, so the cutoff and the intensity of HHG are reduced. The intensity and the modulations of the HHG spectrum are important characters for its application. To reduce the modulations and increase the intensity, we simulate a scheme with the FWHM of the pulse even shorter than one cycle, e.g., $\tau = 5$ fs and $\varphi = 0$. Other parameters are the same as the above scheme. The dash dotted blue line in Fig. 1 shows that a super-continuum plateau structure is obtained with a cutoff of about the 320th order. The intensity of the HHG spectrum is higher than that for the case of $\tau = 5$ fs. Continuum plateau imply that little interference exists in the region from 90th to 320th.

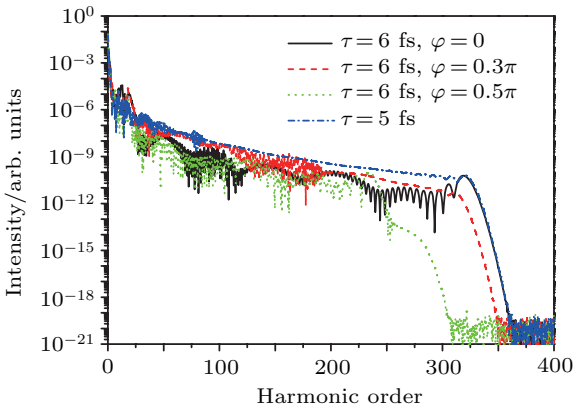


Fig. 1. (color online) The spectrum of HHG obtained by few-cycle femtosecond laser pulse.

To study the spatial distribution in HHG, we demonstrate the modulus square of the Fourier transform of Eq. (7). Figure 2(a) shows the result for the case of $\tau = 6$ fs, $\varphi = 0$. It is indicated that the contribution to HHG is weak around the position $x = 0$ and the equilibrium internuclear position

$x = \pm 3.5$ a.u., which is consistent with the results demonstrated in Ref. [14]: the electron cannot recombine to the middle of the two nuclei and cannot locate within the nucleus region. The intensity of HHG from the nucleus along the positive-x direction is as strong as that from the nucleus along the negative-x direction under the 225th order, but weaker near the cut-off area, e.g., from 225th to 320th. Harmonic emission from two contiguous nuclei may lead to interference, which is unexpected in some cases such as producing attosecond pulses. How to eliminate the spatial interference is a topic which needs to be investigated.

For the case of $\tau = 6$ fs, $\varphi = 0.3\pi$, figure 2(b) shows that the contribution to the HHG is from both nuclei below the 200th order and the HHG is mainly from the nucleus along the negative-x direction greater than the 200th order. The interference of HHG from the two nuclei is eliminated, so there is little modulation in the region from the 200th order to the 310th order. When the CEP is set to be $\varphi = 0.5\pi$, the intensity of HHG from the nucleus along the positive-x direction is as strong as that from the nucleus along the negative-x direction, as shown in Fig. 2(c). These characters correspond to the structure of HHG spectrum shown in Fig. 1. The result is shown in Fig. 2(d) for the case of $\tau = 5$ fs, $\varphi = 0$. We can see that the contribution to the HHG is from both nuclei below the 90th order; however, the contribution to the HHG is mainly from the nucleus along the negative-x direction greater than the 90th order. The spatial contribution in HHG is restrained well for the case of $\tau = 5$ fs. We try to use other internuclear distances to analyze the spatial distribution of HHG. For the case of small internuclear distance, e.g., $R = 2$, the spatial distribution of HHG was hardly restrained. Both of the nuclei contributed to the HHG. For the case of large internuclear distance, the result was similar to the discussion in our manuscript. Further analysis is needed to explain the physical mechanism.

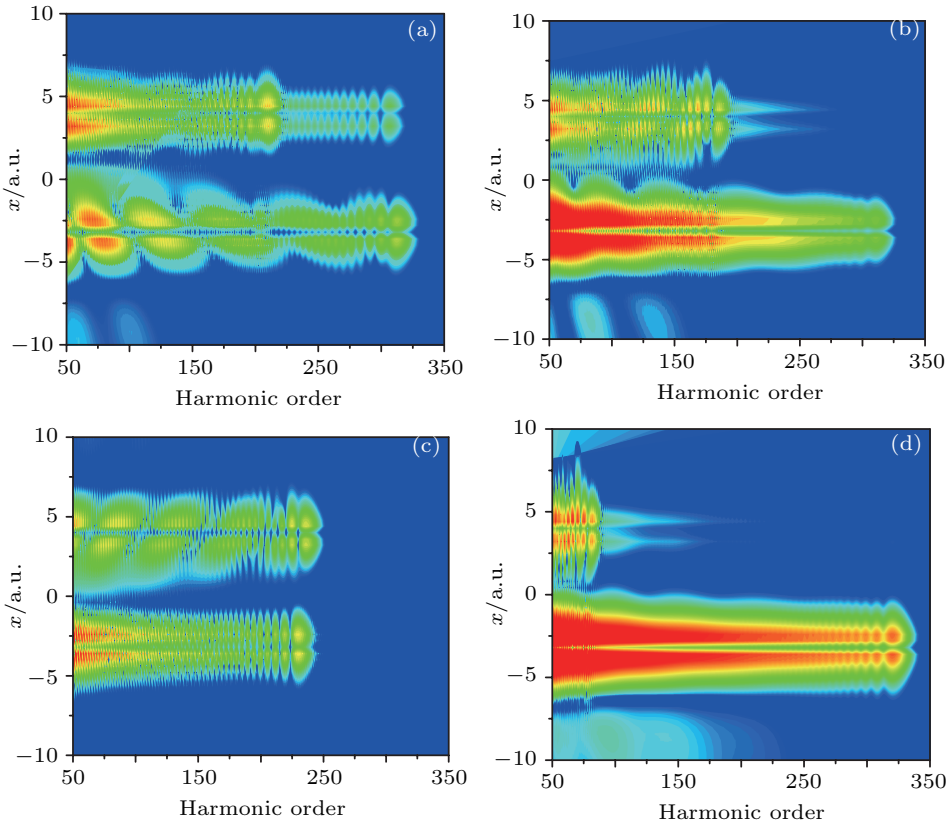


Fig. 2. (color online) Spatial distribution in HHG with different FWHMs. (a) $\tau = 6$ fs, $\varphi = 0$, (b) $\tau = 6$ fs, $\varphi = 0.3\pi$, (c) $\tau = 6$ fs, $\varphi = 0.5\pi$, (d) $\tau = 5$ fs, $\varphi = 0$.

The time–frequency analysis is calculated by using the Morlet wavelet transformation of Eqs. (4) and (5) to illustrate the physical mechanism. Figure 3(a) shows the time–frequency analysis along the negative-x direction for the case of $\tau = 6$ fs and $\varphi = 0$. Two quantum peaks which are labeled as A_1 and B_1 contribute to the HHG in the period of 2.5–4.0 o.c., and each peak has two quantum paths, i.e., the short and long quantum path. The modulations of the HHG are attributed to the interference of quantum paths. Both short and long quantum paths in A_1 and B_1 contribute to the HHG below the 125th order. However, only peak A_1 contributes to HHG in the plateau from the 125th to the 320th order and the intensity of the long quantum path is weak. This can explain the phenomenon that there are more modulations in the low order region than in the high order region in the plateau. Figure 3(b) shows the time–frequency analysis along the positive-

x direction and the characteristic is similar to that shown in Fig. 3(a). The intensity of peak A_2 near the cutoff region is a little weaker than that of peak A_1. This explains why the intensity of HHG from the nucleus along the positive-x direction is weaker than that along the negative-x direction near the cut-off area, as discussed in Fig. 2(a).

Figure 3(c) shows the time–frequency analysis along the negative-x direction for the case of $\tau = 5$ fs and $\varphi = 0$. Both short and long quantum paths can be observed in the plateau region (see the peak A_3), and the intensity of the long quantum path is weaker than that of the short one. In the region below the 90th order, both peak B_3 and peak A_3 contribute to the HHG. Figure 3(d) shows the case along the positive-x direction. Both short and long quantum paths can be observed in peak B_4 and the peak harmonic order is about the 90th order, which corresponds to the structure of HHG spectra in the low-order region. There is only a short quantum path in peak A_4 and the intensity is very weak near the cutoff region. These results correspond to the character that the harmonic near the cutoff region is mainly contributed by the nucleus along the negative-x direction, as shown in Fig. 2(b).

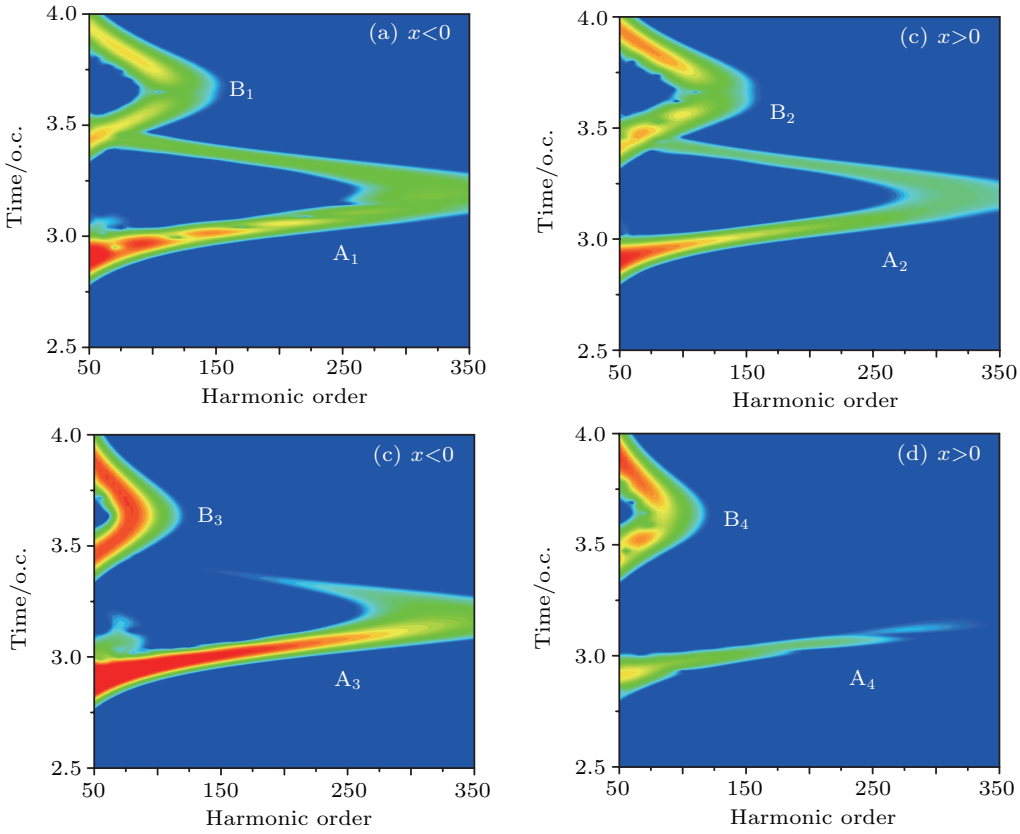


Fig. 3. (color online) Time–frequency analysis by using transformation of the dipole acceleration in Eqs. (4) and (5). (a), (b) $\tau = 6$ fs, $\varphi = 0$; (c), (d) $\tau = 5$ fs, $\varphi = 0$. (a), (c) Time–frequency distribution from Eq. (4); (b), (d) time–frequency distribution from Eq. (5).

The temporal evolution of the electron probability density is demonstrated to illustrate the physical mechanism. The nucleus contributing to the HHG can be investigated by the electron probability density. If the electron probability density is low near the nucleus along the positive-x direction, the electron is seldom transited back to the ground state of that nucleus, then we can obtain that the HHG is mainly from the nucleus along the negative-x direction for this case. For the case of $\tau = 6$ fs and $\varphi = 0$, the results are shown in Figs. 4(a)–4(d). At $T = 2.0$ o.c., two circle peaks with centers located at $(-3.5, 0)$ and $(3.5, 0)$ are formed, and the radius is about 3.5 a.u., the electron distributes uniformly near both of the nuclei. At $T = 2.6$ o.c., the radius of the circle near the nucleus along the positive-x direction is about 7.0 a.u., which is larger than that near the other nucleus. At $T = 3.0$ o.c., the electron density distribution has three peaks with the center about $(-7.0, 0)$, $(-2.5, 0)$, and $(3.1, 0)$, and the probability density distribution in the y direction is larger than the above two cases. More than two thirds of the probability is near the nucleus along the negative-x direction. At $T = 3.2$ o.c., the probability density distribution mainly has two separate peaks with the center about $(-3.8, 0)$ and $(3.1, 0)$, and the radius and the peak near the nucleus along the negative-x direction are larger than near the other nucleus. Those results are consistent with the discussion in Figs. 3(a) and 3(b), the characteristics are similar and the intensity of quantum peak A_2 is a little weaker than that of peak A_1.

For the case of $\tau = 5$ fs and $\varphi = 0$, the electron probability densities are shown in Figs. 4(e)–4(h). Figure 4(e) shows the electron distribution at $T = 2.0$ o.c. We can see that the

electron distributes uniformly near both nuclei, which is similar to that shown in Fig. 4(a). At $T = 2.6$ o.c., figure 4(f) shows that the probability of the electron near the nucleus along the positive-x direction is less than the other nucleus. At $T = 3.0$ o.c., figure 4(g) shows that there is only one peak with the center about $(-3.8, 0)$, and the probability density distribution in the y direction is less than the case of $\tau = 6$ fs. At $T = 3.2$ o.c., the electron distribution has one circle peak with the center of $(-3.5, 0)$ and there is scarce probability near the nucleus along the positive-x direction. The probability density of an electron located near the nucleus along the negative-x direction explains the phenomenon of quantum peak A_4 being weaker than quantum peak A_3, as shown in Figs. 3(a) and 3(b). In a word, the spatial distribution in HHG is restrained by the electron location.

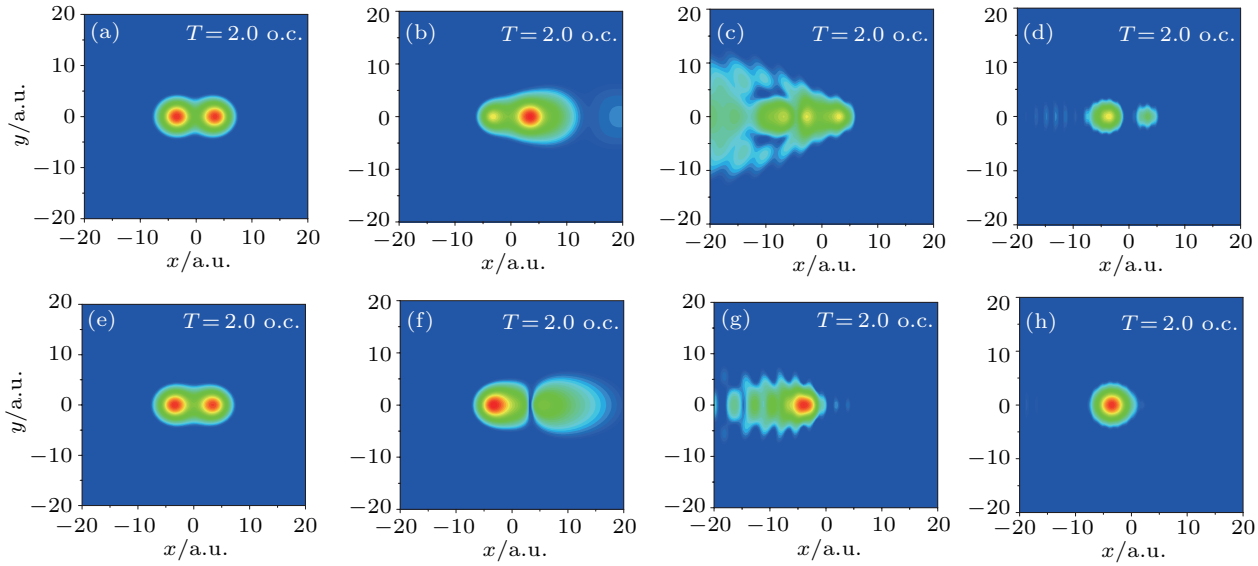


Fig. 4. (color online) The electron probability density evolution in different times. (a)–(d) $\tau = 6$ fs, $\varphi = 0$, (e)–(h) $\tau = 5$ fs, $\varphi = 0$.

4. Conclusion

In conclusion, we theoretically investigate the HHG process from a two-dimensional model of a hydrogen molecular ion. We find a scheme to restrain the spatial distribution in HHG near the cutoff area: by adding a 5 fs linearly polarized laser pulse in the direction of molecular orientation, the harmonic spectra are mainly contributed from the nucleus along the negative-x direction in the region from 90th to 320th. The physical mechanism of the phenomenon is explained by the electron location and the time–frequency analysis. To explain the physical mechanism, we give the probability density of an electron wave packet in different times and find that the probability density of the electron wave packet is mainly located near the nucleus along the negative-x direction from 3.0 o.c. to 3.2 o.c. for the case of $\tau = 5$ fs and $\varphi = 0$. The work in this paper has potential applications for further understanding the quantum interference effect and obtaining isolated attosecond pulse.

References

[1] Winterfeldt C, Spielmann C and Gerber G 2008 *Rev. Mod. Phys.* **80** 117
[2] Heyl C M, Rudawski P, Brizuela F, Bengtsson S N, Mauritsson J and L'Huillier A 2014 *Phys. Rev. Lett.* **112** 143902
[3] Niikura H, Dudovich N, Villeneuve D M and Corkum P B 2010 *Phys. Rev. Lett.* **105** 053003
[4] Klaiber M, Hatsagortsyan K Z, Müller C and Keitel C H 2008 *Opt. Lett.* **33** 411
[5] Hentschel M, Kienberger R, Spielmann Ch, *et al.* 2001 *Nature* **414** 509
[6] Krausz F and Ivanov M 2009 *Rev. Mod. Phys.* **81** 163
[7] Corkum P B 1993 *Phys. Rev. Lett.* **71** 1994
[8] Schafer K J, Yang B, DiMauro L and Kulander K C 1993 *Phys. Rev. Lett.* **70** 1599
[9] He X, Miranda M, Xchwenke J, *et al.* 2009 *Phys. Rev. A* **79** 063829
[10] Heyl C M, Güdde J, Höfer U and L'Huillier A 2011 *Phys. Rev. Lett.* **107** 033903
[11] Jin C, Stein G J, Hong K H and Lin C D 2015 *Phys. Rev. Lett.* **115** 043901
[12] He L, Lan P, Zhang Q, Zhai C, Wang F, Shi W and Lu P 2015 *Phys. Rev. A* **92** 043403
[13] Lambert G, Andreev A, Gautier J, *et al.* 2015 *Sci. Rep.* **5** 7786
[14] Zhang J, Ge X L, Wang T, *et al.* 2015 *Phys. Rev. A* **92** 013418
[15] Zhang J, Liu H F, *et al.* 2016 *Chin. Phys. B* **25** 053202
[16] Lan P, Takahashi E J and Midorikawa K 2012 *Phys. Rev. A* **86** 013418
[17] Rathje T, Sayler A M, Zeng S, *et al.* 2013 *Phys. Rev. Lett.* **111** 093002
[18] Liu K, Zhang Q, Lan P and Lu P 2013 *Opt. Express* **21** 5107
[19] Roudnev V, Esry B and Ben-Itzhak I 2004 *Phys. Rev. Lett.* **93** 163601
[20] Kling M, Siedschlag C, Verhoef A, *et al.* 2006 *Science* **312** 246
[21] He F, Ruiz C and Becker A 2007 *Phys. Rev. Lett.* **99** 083002
[22] Singh K P, He F, Ranitovic P, *et al.* 2010 *Phys. Rev. Lett.* **104** 023001
[23] He F 2012 *Phys. Rev. A* **86** 063415
[24] Sukharev M E and Krainov V P 2000 *Phys. Rev. A* **62** 033404
[25] Xue S, Du H, Xia Y and Hu B 2015 *Phys. Rev. A* **92** 013420
[26] Miller M R, Jaroń-Becker A and Becker A 2016 *Phys. Rev. A* **93** 013406
[27] Li L Q, Xu Y Y and Miao X Y 2016 *J. At. Mol. Sci.* **7** 1
[28] Salières P, Ditmire T, Perry M D, *et al.* 1996 *J. Phys. B: At. Mol. Opt. Phys.* **29** 4771
[29] Jin C, Stein G J, Hong K H and Lin C D 2015 *Phys. Rev. Lett.* **115** 043901
[30] Xia C L and Miao X Y 2016 *J. At. Mol. Sci.* **7** 17
[31] Xia C L, Zhang G T, Wu J and Liu X S 2010 *Phys. Rev. A* **81** 043420
[32] Feit M D, Fleck Jr J A and Steiger A 1982 *J. Comput. Phys.* **47** 412
[33] Lein M, Hay N, Velotta R, *et al.* 2002 *Phys. Rev. Lett.* **88** 183903
[34] Wang J, Chen G, Guo F M, *et al.* 2013 *Chin. Phys. B* **22** 033203